Geomechanics and Engineering, *Vol. 41, No. 4 (2025) 407-417*
https://doi.org/10.12989/gae.2025.41.4.407

Three-dimensional seismic stability analysis of slopes with linearly increasing undrained shear strength

Yunwei Shi[a], Xianqi Luo* and Pingfan Wang[b]

School of Ocean & Civil Engineering, Shanghai Jiao Tong University,
800 Dongchuan Road, Minhang District, Shanghai, China

(*Received January 7, 2025, Revised April 3, 2025, Accepted April 7, 2025*)

Abstract. Undrained stability of slopes has long been of interest to the community of geotechnical engineering due to its practical importance. However, the role of the undrained shear strength c_u in the seismic stability and failure geometry of slopes under three-dimensional (3D) condition has not been fully understood. Therefore, this study adopts a modified 3D rotational failure mechanism to develop the upper bound solution to the stability number N_s for slopes with linearly increasing c_u with depth based on the kinematic approach of limit analysis. The seismic force is included using the pseudo-static method. Three types of failure mechanisms, i.e., the toe failure, face failure and below-toe failure are considered to capture the critical condition. Stability charts that cover a wide range of parameters and representative failure surfaces are then developed to illustrate the influence of key factors. Results show that the stability and failure geometry of slopes are significantly influenced by the variation ratio of c_u with depth. The most significant outcome is that an increase in the horizontal seismic coefficient k_h leads to a shallower critical failure surface when the slope with a large variation ratio of c_u is constrained within a narrow width.

Keywords: 3D slope stability; failure mechanism; limit analysis; undrained shear strength

1. Introduction

Seismic hazards can lead to significant consequences, such as landslides and liquefaction of soils (Mase *et al*. 2020, 2021, 2022, 2024), which may induce severe damage to properties, thus assessing seismic slope stability is of concern in geotechnical engineering. Over the past decades, the stability of slopes has been assessed using various numerical methods, such as finite element method (Ukritchon *et al*. 2020, Naeij *et al*. 2021, Satyanaga *et al*. 2022, Petchkaew *et al*. 2023a, 2023b, Wang *et al*. 2024), discrete element method (Bonilla-Sierra *et al*. 2015, Weng *et al*. 2019, Gao *et al*. 2021, Ajith *et al*. 2024), material point method (Bhandari *et al*. 2016, Feng and Xu 2021, Wang *et al*. 2025) and smooth particle hydrodynamics (Ray *et al*. 2019, Zhang *et al*. 2024). Numerical methods have advantages in dealing with slopes with complicated geometric forms and loading conditions, therefore they are extensively adopted for case studies (Bi *et al*. 2019, Azarafza *et al*. 2021, Tran *et al*. 2019, 2023). The limitation of numerical methods lies in the intensive computational effort when carrying out parametric studies. In contrast, analytical approaches including the limit-equilibrium method (Deng *et al*. 2019, Chaudhary *et al*. 2024) and limit analysis method (Rao *et al*. 2021, Chehade *et al*. 2022) are more convenient for performing parametric studies. The limit equilibrium method is the most frequently used method in engineering practice. Despite its popularity, some limitations still exist in the assumptions with respect to the inter-column forces, the direction of resultant shear resistance and moment equilibrium conditions (Zhou and Qin 2020). The limit analysis method offers a rigorous upper/lower bound for slope stability problems by constructing the kinematically admissible velocity field/statically admissible stress field (Chen 1975). A rigorous upper bound solution to the critical slope height or the factor of safety can be obtained by assuming a reasonable slip surface.

When assessing the undrained stability of slopes or excavations in normally consolidated clays, the undrained shear strength c_u was generally assumed to linearly increase with depth (Hunter and Schuster 1968, Kumar *et al*. 2014). Koppula (1984) assessed the stability of slopes with linearly increasing c_u, where the undrained strength is positive finite on the top surface of the slope. The results demonstrated that the variation ratio of c_u significantly affects the slope stability and the depth of failure surface. Griffiths and Yu (2015) investigated the influence of a firm stratum on the stability and failure surface of slopes with linearly increasing c_u. The zero strength at the crest level was also examined. Some novel results were obtained compared with those of Hunter and Schuster (1968). Li *et al*. (2018) presented a procedure for analyzing the impact of tension crack on the stability of slopes with linearly increasing c_u. It was found that the effect of tension crack on the undrained slope stability is significant under the seismic condition. Griffith and Matin (2020) investigated the failure

*Corresponding author, Professor
E-mail: luoxianqi402@yeah.net
[a]Ph.D. Student
E-mail: yunwei_shi@yeah.net
[b]Ph.D. Student
E-mail: pingfan.wang@sjtu.edu.cn

ISSN: 2005-307X (Print), 2092-6219 (Online)

mechanisms and stability of relatively flat undrained slopes by three different methods, i.e., finite-element limit analysis (FELA), elastic-plastic finite element (EPFE) and classical slip-circle analysis. It was found that the classical slip-circle analysis cannot give reasonable results for relatively flat slopes (slope angle $\beta \leq 10°$), especially when the depth ratio is small. In recent years, the influence of the variation of c_u in the lateral direction on slope stability under static condition has also been investigated (Hossley and Leshchinsky 2019, Ke *et al*. 2021, Shi *et al*. 2022). Three-dimensional analyzes were also carried out (Shu *et al*. 2023). Li *et al*. (2009) produced stability charts for 3D undrained slopes, however, the failure mechanisms were not indicated in these charts. Zhou *et al*. (2019) further extended these charts to include the horizontal seismic excitation. Shu *et al*. (2023) proposed a 3D slope reliability analysis approach that can fully consider the spatial variability of undrained soil properties within the framework of random field theory and Monter Carlo simulation. The results indicated that for larger slope inclinations, the greater the undrained shear strength, the more likely the sliding surface displays a deep toe circle or a toe circle. Hong-in *et al*. (2023) investigated the 3D seismic and failure mechanism of undrained clay slopes based on FELA. A predicted equation that can effectively estimate the stability number was developed. Although much progresses have been made, the effect of the linearly increasing c_u on the failure geometry of slopes were only investigated under specific scenarios. The influence of the linearly increasing c_u on the 3D stability and failure geometry of slopes under seismic excitation remains unclear.

Therefore, the 3D seismic stability of slopes with linearly increasing undrained shear strength c_u is investigated based on the kinematic approach of limit analysis in the present work. The horizontal seismic force is included using the pseudo-static method. The upper bound solution to the stability number N_s is obtained based on the virtual work principle. The failure mechanisms including the below-toe failure, toe failure and face failure are taken into account to capture the most critical condition. A series of charts and representative failure surfaces are developed to illustrate the influence of key parameters on the slope stability and failure geometry.

2. Kinematic approach of limit analysis and its application

The application of kinematic approach of limit analysis in geotechnical engineering was presented systematically by Chen (1975). The results obtained by the kinematic approach of limit analysis in slope stability analysis have been proved to be credible (Chen 1975, Zhang *et al*. 2016). In the framework of the kinematic approach of limit analysis, Chen (1975) adopted the log-spiral rotational failure surface to assess 2D slope stability. With respect to the 3D analysis, Michalowski and Drescher (2009) proposed a horn-like failure mechanism (as depicted in Fig. 1) which has been the most commonly used mechanism

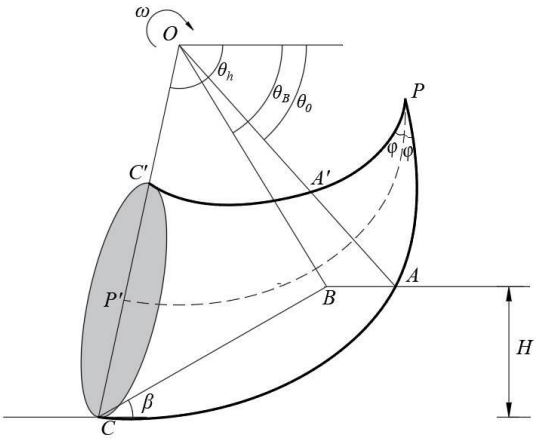

Fig. 1 Failure mechanism proposed by Michalowski and Drescher (2009)

during the last decade (Yang and Pan 2015, Wang *et al*. 2019, Karrech *et al*. 2022), however, the geometric constraint used in their research limits the range of admissible mechanisms. Park and Michalowski (2018) further modified the failure mechanism proposed by Michalowski and Drescher (2009) to lift the geometric constraint, and this modified failure mechanism is adopted to develop the upper bound solution in current work.

3. Assumptions

To facilitate the 3D stability analysis of slopes with linearly increasing undrained shear strength, following assumptions are made:

1) linear Mohr-Coloumb failure criterion is satisfied.

2) soils are ideal rigid and perfectly plastic with an associated normality rule.

4. Methodologies

4.1 Undrained shear strength profile

The undrained shear strength profile is depicted in Fig.2. In the figure, the slope with height H and angle β is made of soil with a unit weight γ. The soil exhibits a linear increase in the undrained shear strength with depth. The undrained shear strength at any point can be defined as

$$c_u(z) = c_{u0} + kz \tag{1}$$

where z is the depth of a given point measured form the slope top surface; k is the strength gradient in the depth direction; c_{u0} is the undrained shear strength at the slope crest level (z=0).

In order to facilitate the parametric study, a dimensionless strength gradient parameter M introduced by Hunter and Schuster (1968) is adopted:

$$M = \frac{c_{u0}}{kH} \tag{2}$$

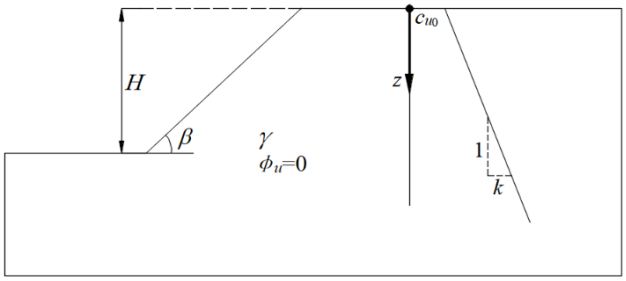

Fig. 2 Problem depiction and notation

4.2 Failure mechanism

As shown in Fig. 3, the failure mechanism becomes a torus for the undrained analysis. Note that when dealing with soils with varied friction angle, the failure mechanism is no longer valid. Three types failure mechanism, i.e., the toe failure, face failure and below-toe failure are considered. The below-toe failure becomes the toe failure when $\beta' = \beta$ (Fig. 3(a)). And the face failure is a special case of toe failure with a smaller slope height H' (Fig. 3(b)). The following equations are formulated based on the below-toe failure mechanism.

The trace of the failure mechanism on the symmetry plane is described by two circular arc AD and AD', which can be respectively expressed as

$$r = r_0 \tag{3}$$

$$r' = r_0' \tag{4}$$

The mechanism is generated by rotating a circle defined by the arc given in Eqs. (3)-(4) around the axis passing through the rotation center O. The distance from the rotation center O to the axis of the torus r_m and the radius of the circle R can be expressed as

$$r_m = \frac{r_0 + r_0'}{2} \tag{5}$$

$$R = \frac{r_0 - r_0'}{2} \tag{6}$$

In the polar coordinate system, the contour of the slope can be described as a piece-wise function

$$r_s(\theta) = \begin{cases} \dfrac{r_0 \sin\theta_0}{\sin\theta}, & \theta_0 < \theta \le \theta_B \\ \dfrac{r_0 \sin(\beta+\theta_h)}{\sin(\beta+\theta)}, & \theta_B < \theta \le \theta_C \\ \dfrac{r_0 \sin\theta_h}{\sin\theta}, & \theta_C < \theta \le \theta_h \end{cases} \tag{7}$$

The z coordinate for the c_u profile can be expressed as

$$z = r_0(\sin\theta - \sin\theta_0) \tag{8}$$

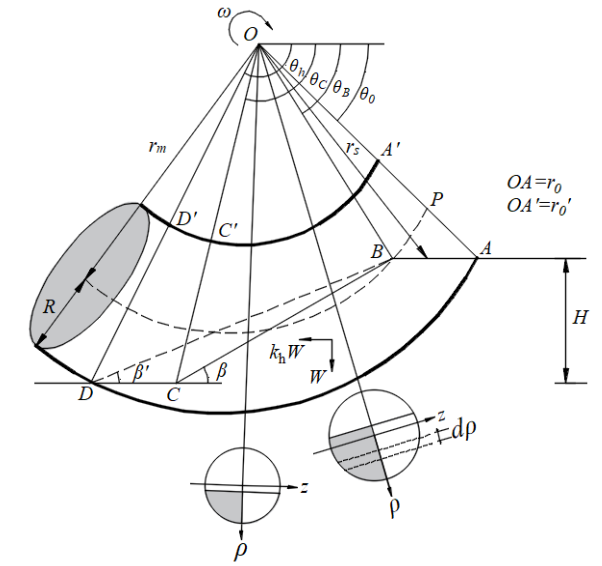

(a) Below-toe failure

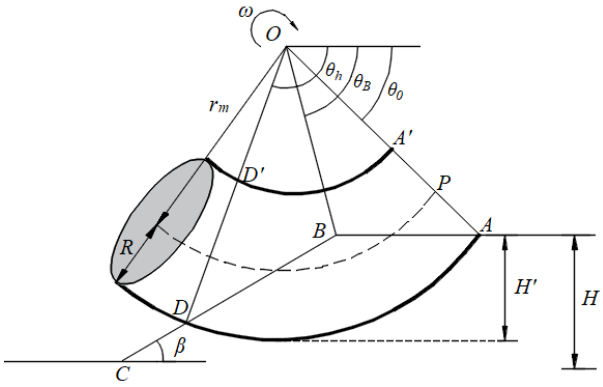

(b) Face failure

Fig. 3 Three-dimensional undrained failure mechanism

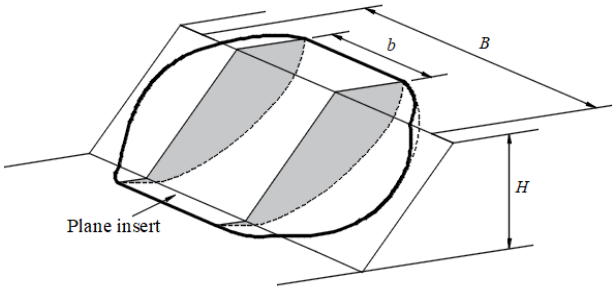

Fig. 4 Mechanism with plane insert

Fig. 4 shows the mechanism for the slope with finite width B modified with a block of width b. When b approaches infinity, the 3D failure mechanism is transformed to the 2D failure mechanism. For a 2D undrained analysis, the depth of the failure mechanism in gentle slopes tends to infinity (Michalowski 2002), hence a firm stratum should be introduced to obtain more rational results. It is noted that this failure mechanism in only valid under undrained condition. If the heterogeneity of the internal friction angle needs to be considered, new failure mechanisms should be developed.

4.3 Solution for the stability number

Based on the failure mechanism depicted in Fig. 3(a), the procedure to determine the stability number N_s will be presented in the following.

For the torus, the work rate done by soil weight can be expressed as

$$W_{\gamma}^{3D}=2\omega\gamma\int_{\theta_0}^{\theta_h}\int_{r_s}^{r}\rho^2\cos\theta\sqrt{R^2-\left(\rho-r_m\right)^2}\,d\rho d\theta \tag{9}$$

The vertical acceleration has little effect on slope stability and is ignored herein (Huang *et al*. 2023). The work rate done by the horizontal seismic force can be obtained based on the pseudo-static method

$$W_{k_h}^{3D}=2\omega\gamma k_h\int_{\theta_0}^{\theta_h}\int_{r_s}^{r}\rho^2\sin\theta\sqrt{R^2-\left(\rho-r_m\right)^2}\,d\rho d\theta \tag{10}$$

where k_h is the horizontal seismic coefficients

The work rate done by soil weight for the plane insert can be expressed as

$$W_{\gamma}^{2D}=\gamma\omega r_0^3\left(f_1-f_2-f_3-f_4\right) \tag{11}$$

where f_1-f_4 can be defined as:

$$f_1=\frac{\sin\theta_h-\sin\theta_0}{3} \tag{12}$$

$$f_2=\frac{1}{6}\frac{L}{r_0}\sin\theta_0\left(2\cos\theta_0-\frac{L}{r_0}\right) \tag{13}$$

$$f_3=\frac{1}{6}\left[\sin\left(\theta_h-\theta_0\right)-\frac{L}{r_0}\sin\theta_h\right]\left(\cos\theta_0+\cos\theta_h-\frac{L}{r_0}\right) \tag{14}$$

$$\begin{aligned}f_4=&\frac{1}{2}\left(\frac{H}{r_0}\right)^2\left[\left(\cot\beta'-\cot\beta\right)\cos\theta_0\right.\\&\left.-\frac{L}{r_0}-\frac{H}{3r_0}\left(\cot\beta'+\cot\beta\right)\right]\end{aligned} \tag{15}$$

where H/r_0 and L/r_0 can be defined as

$$\frac{H}{r_0}=\sin\theta_h-\sin\theta_0 \tag{16}$$

$$\frac{L}{r_0}=\frac{\sin\left(\theta_0+\beta'\right)-\sin\left(\theta_h+\beta'\right)}{\sin\beta'} \tag{17}$$

The work rate done by the horizontal seismic force for the plane insert can be expressed as

$$W_{k_h}^{2D}=\gamma\omega r_0^3 k_h\left(f_5-f_6-f_7-f_8\right) \tag{18}$$

where f_5-f_8 can be defined as

$$f_5=\frac{\cos\theta_0-\cos\theta_h}{3} \tag{19}$$

$$f_6=\frac{1}{3}\frac{L}{r_0}\sin\theta_0^2 \tag{20}$$

$$f_7=\frac{1}{6}\left[\sin(\theta_h-\theta_0)-\frac{L}{r_0}\sin\theta_h\right]\left(\sin\theta_0+\sin\theta_h\right) \tag{21}$$

$$f_8=\frac{1}{2}\left(\frac{H}{r_0}\right)^2\left(\cot\beta'-\cot\beta\right)\left(\frac{2}{3}\frac{H}{r_0}+\sin(\theta_0)\right) \tag{22}$$

Then the total external work rate can be expressed as

$$W_{tot}=W_{\gamma}^{3D}+W_{k_h}^{3D}+b\cdot\left(W_{\gamma}^{2D}+W_{k_h}^{2D}\right) \tag{23}$$

Due to the rigid body assumption, the internal energy dissipation inside the sliding body is ignored. The internal energy dissipation rate along the failure surface of the torus can be expressed as

$$D^{3D}=2c_u\left(x,z\right)\omega\int_{\theta_0}^{\theta_h}\int_{r_s}^{r}\rho^2\frac{R}{\sqrt{R^2-\left(\rho-r_m\right)^2}}\,d\rho d\theta \tag{24}$$

The internal energy dissipation rate of the plane insert can be expressed as

$$D^{2D}=\int_{\theta_0}^{\theta_h}c_u\left(x,z\right)vr_0\,d\theta=\omega r_0^2\int_{\theta_0}^{\theta_h}c_u\left(x,z\right)d\theta \tag{25}$$

Then the total internal energy dissipation rate can be expressed as

$$D_{\text{int}}=D^{3D}+b\cdot D^{2D} \tag{26}$$

Based on the gravity increase method, the safety factor can be defined as the ratio of the total energy dissipation rate to the total external work rate (Yang and Li 2018)

$$F_s=\frac{D_{\text{int}}}{W_{tot}} \tag{27}$$

Therefore, the stability number Ns can be obtained

$$N_s=F_s\cdot\frac{\gamma}{k} \tag{28}$$

To yield the least upper bound solution to N_s, an optimization procedure with respect to the unknown parameters (θ_0, θ_h, r'/r and β') was coded in MATLAB. The optimization procedure proposed by Chen (1992) was adopted herein. An initial estimate of the unknown parameters can be obtained by the random search method, then the global minimum can be searched by the optimization procedure.

5. Comparison

To validate the robustness of the developed solution and the optimization procedure, the solution in the study is degraded into the homogeneous condition. Herein the calculated dimensionless critical slope heights $\gamma H/c_{u0}$ which can be obtained by equating Eq. (23) to Eq. (26) are

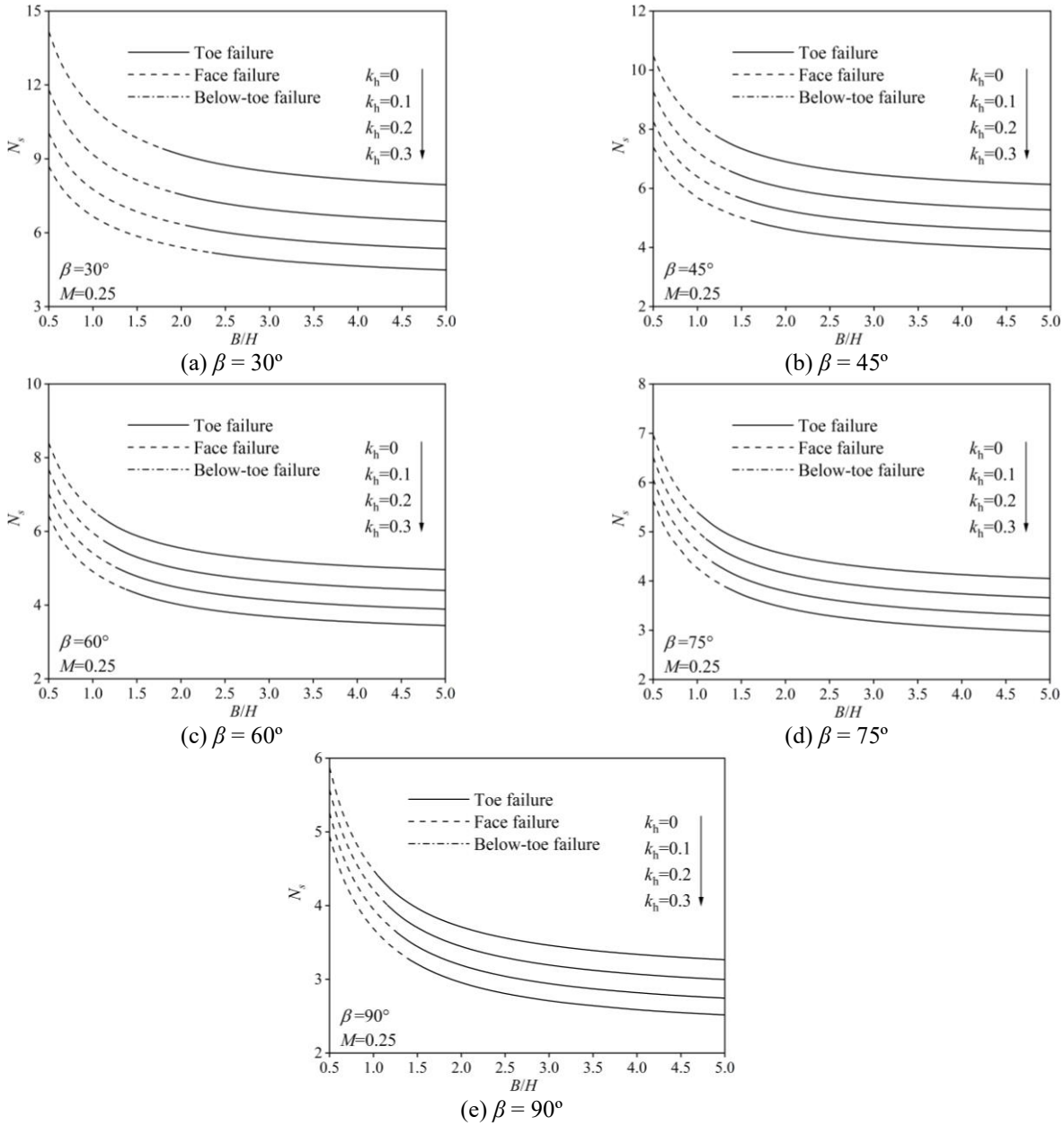

(a) β = 30º (b) β = 45º

(c) β = 60º (d) β = 75º

(e) β = 90º

Fig. 5 Variation of stability number N_s with width-to-height ratio B/H for M = 0.25

Table 1 Comparison of results

		$\gamma H/c_{u0}$	
β	B/H	This study	Park and Michalowski (2018)
30º	0.5	16.644	16.645
30º	1	10.792[a]	10.797[a]
30º	3	7.398[a]	7.389[a]
45º	0.5	12.812	12.789
45º	1	9.020[a]	9.021[a]
45º	3	6.795[a]	6.783[a]
60º	0.5	10.865	10.860
60º	1	7.821	7.821
60º	3	6.022	6.022

[a]: Below-toe failure

compared with those obtained by Park and Michalowski (2018), as shown in Table 1. It is clear that the present solution agrees well with the result of Park and Michalowski (2018).

The case of linearly increasing undrained shear strength with c_u = 0 (M = 0) at the slope crest level under 2D condition was examined by Griffiths and Yu (2015). The present solution will become 2D solution when b approaches infinity, then the stability number Ns obtained using the proposed approach are 8.511, 4.106 and 2.563 for β = 15º, 45º and 75º respectively. These results are identical with those obtained by Griffiths and Yu (2015) as indicated in Fig. 7 in their original work. Then the validity of the solution and the optimization procedure is confirmed.

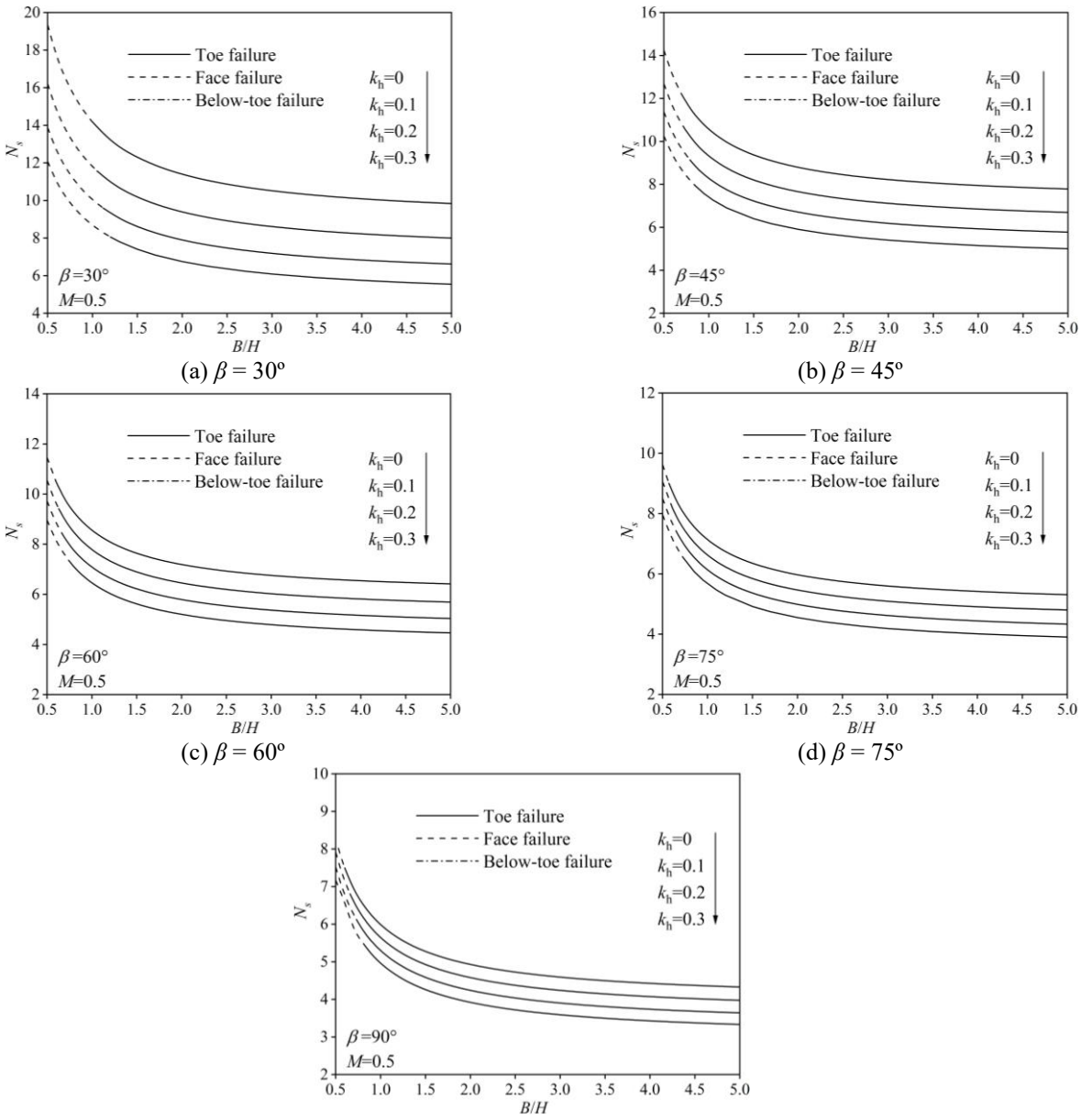

(a) β = 30º (b) β = 45º

(c) β = 60º (d) β = 75º

(e) β = 90º

Fig. 6 Variation of stability number N_s with width-to-height ratio B/H for M = 0.5

6. Results and discussions

To capture the influence of key parameters, i.e., the c_u profile parameter M, horizontal seismic coefficient k_h and width-to-height ratio B/H on the slope stability and failure geometry, a series of charts will be presented in the following section, both the stability number and the failure mechanism are indicated in the figures (solid lines for the toe failure mechanism, dashed lines for the face failure mechanism and dash-dotted lines for the below-toe failure mechanism).

6.1 Slope stability analysis

The obtained stability charts are presented in Figs. 5-8. The plots cover a wide range of slope angel β (30º, 45º, 60º, 75º and 90º), the width-to height ratio B/H varies from 0.5 to 5.

From Figs. 5-8, it can be concluded that as B/H increase from 0.5 to 5, the stability number N_s decreases sharply at early stage, and then the decreasing rate is reduced. Moreover, the increase of M gives rise to an increasing N_s, slopes with smaller B/H ratio are more sensitive to the variation of M. For instance, for a 30º slope with k_h = 0, by increasing M from 0.25 to 0.5, the stability number N_s increases by 36.6% for B/H = 0.5, while an increase of 23.8% is observed for B/H = 5. Manifestly, an increase in k_h leads to a decrease in N_s, and gentler slopes are more sensitive to the variation of k_h. As shown in Figs. 5(a) and 5(d), an increase in k_h from 0 to 0.3 leads to a reduction of

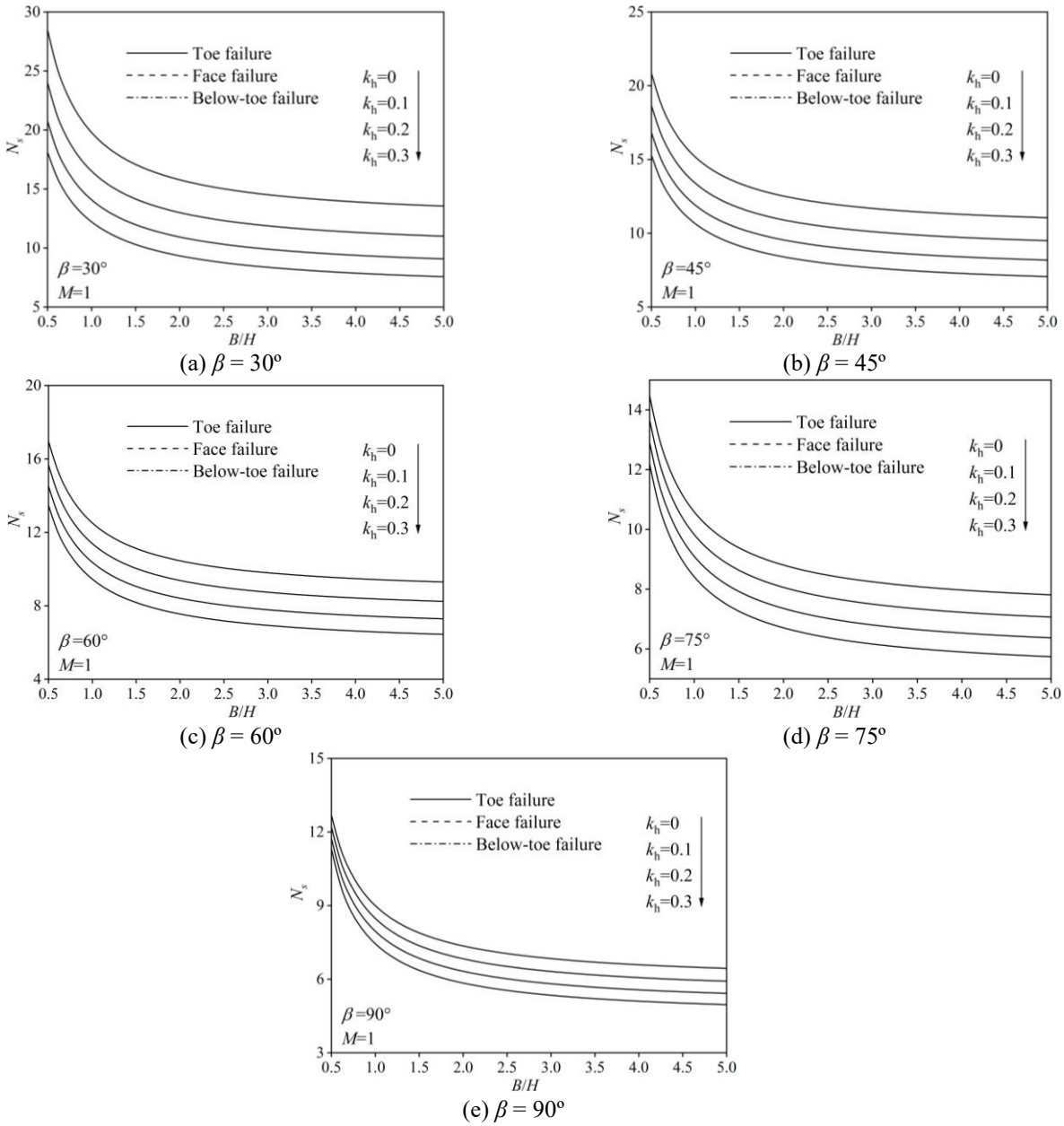

(a) β = 30º (b) β = 45º

(c) β = 60º (d) β = 75º

(e) β = 90º

Fig. 7 Variation of stability number N_s with width-to-height ratio B/H for M = 1

38% and 15% in N_s for 30º and 90º slopes respectively with B/H = 0.5.

As shown in Figs. 5 and 6, when M = 0.25 and 0.5, with the increase of B/H, the failure mode changes from the face failure to the toe failure. An interesting phenomenon can be observed that an increase in k_h leads to more B/H values involved in the face failure mechanism. This phenomenon will be explained later in conjunction with the shape of the failure surface.

Additionally, from the charts, it can be found that the below-tow failure only occurs in gentle slopes when M is large as shown in Fig. 8(a), while the face failure occurs for a wide range of slope angels when M is small. Herein the largest value for M is 2, it is expected that with the further increase of M, the soil strength becomes more uniform, then the failure trends are similar to those observed in homogeneous slope (Gao *et al*. 2013), and thus for a large M value, the below-toe failure is produced in gentle slopes.

6.2 Failure geometry

Selected failure geometries in the symmetry plane for 60º slopes are presented in Fig. 9, the effects of M, B/H and k_h on the critical failure geometries are illustrated in the figure. As can be seen from Fig. 9(a), with the increase of k_h, the failure geometry becomes shallower, while the extent of the failure surface in the horizontal direction becomes wider. This phenomenon is not common since the seismic force tends to make the critical failure surface deeper from the traditional perspective. But it makes sense because when M is small, the variation ratio of c_u in the depth direction is large, then the strength of the upper layer is

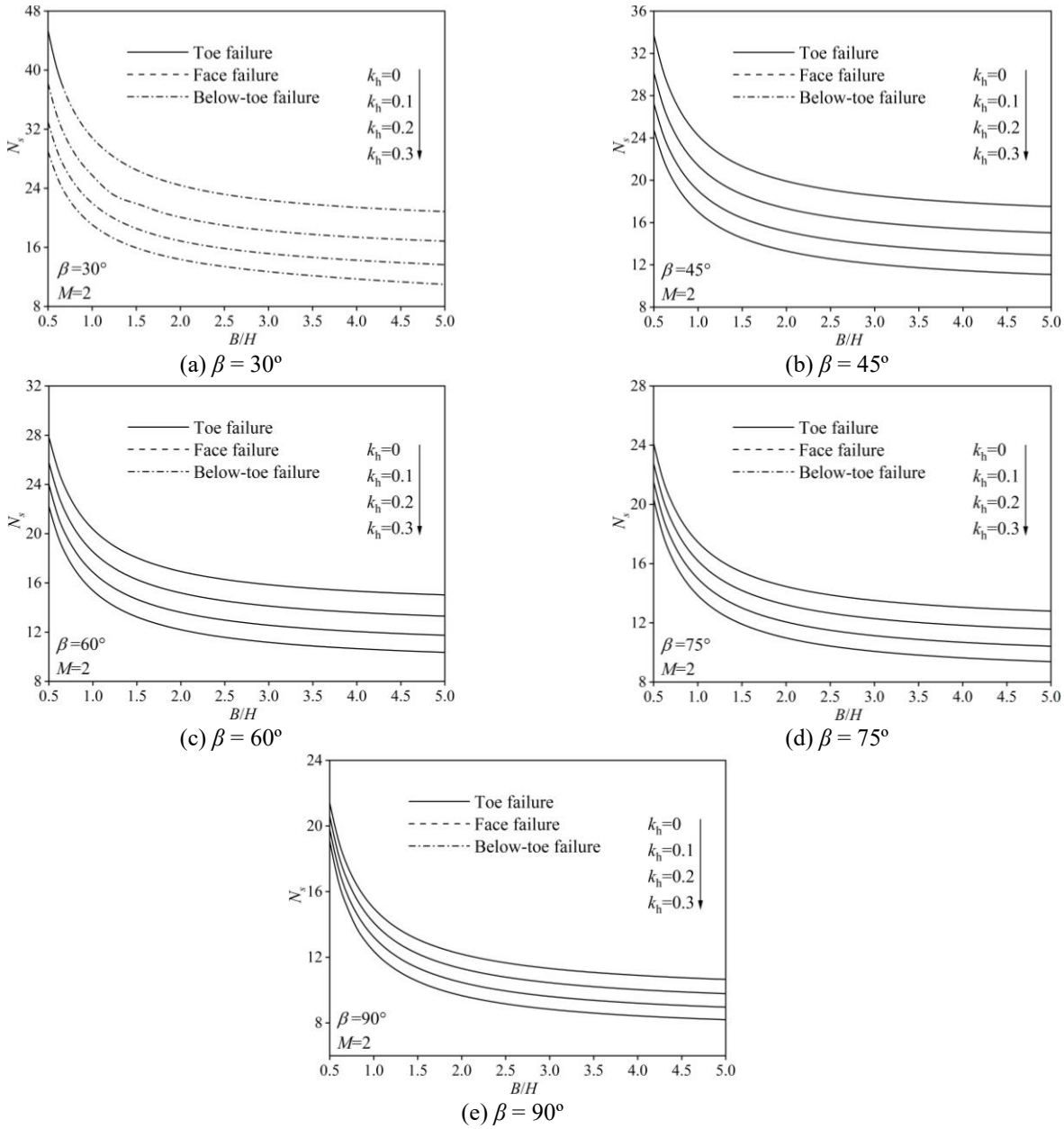

(a) β = 30º (b) β = 45º

(c) β = 60º (d) β = 75º

(e) β = 90º

Fig. 8 Variation of stability number N_s with width-to-height ratio B/H for M = 2

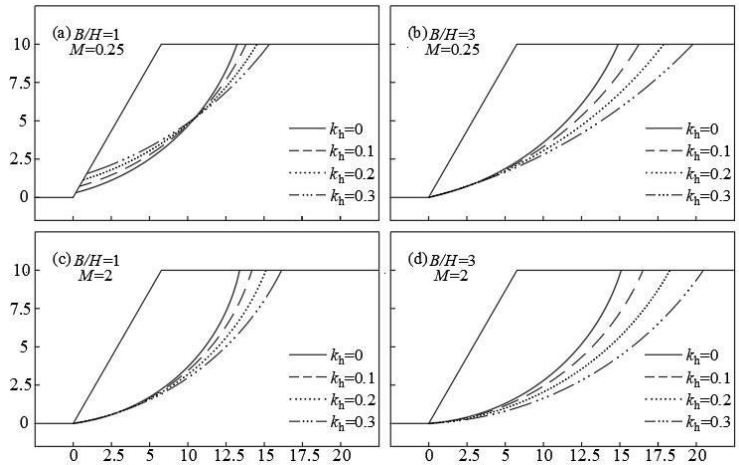

Fig. 9 Failure geometries in the symmetry plane

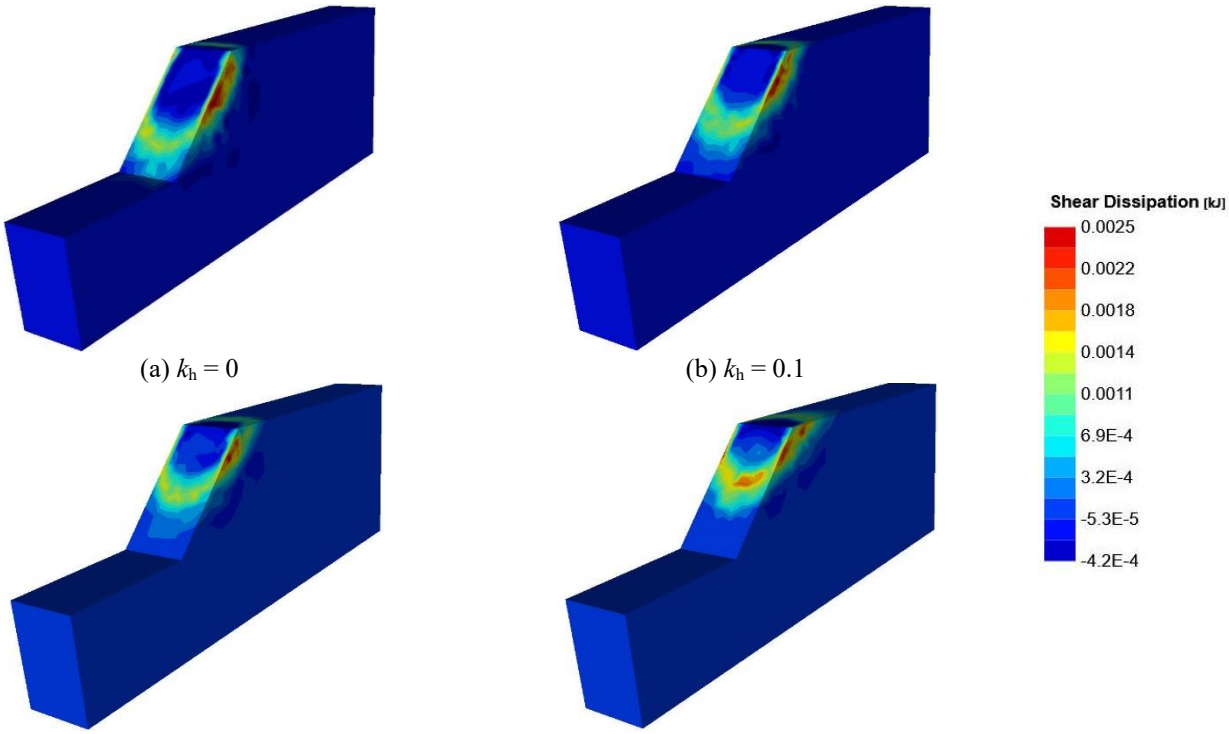

(a) $k_h = 0$ (b) $k_h = 0.1$

(c) $k_h = 0.2$ (d) $k_h = 0.3$

Fig. 10 Three-dimensional failure mechanisms for a slope with $\beta = 45$ °, $B/H = 2/3$ and $M = 0.25$

much weaker than that of the lower layer. In this scenario, compared with a deeper failure surface, a shallower failure surface is much more easily to reach the limit state under the seismic condition. Numerical simulations were also carried out based on the FELA to further verify this conclusion. The detailed numerical scheme can be found in Li *et al*. (2009) and Hong-in *et al*. (2023). Fig. 10 shows the three-dimensional failure mechanisms for a 45º slope with $B/H = 2/3$ and $M = 0.25$ under different horizontal seismic coefficient k_h. It can be seen that with the increase of k_h, the failure mechanism becomes shallower. It is noted that the obtained failure surface gives an estimate of the incipient motion of the slope failure, if a stronger seismic excitation occurs after the initial failure, the secondary failure should be considered (Qin *et al*. 2018).

The aforementioned conclusion holds only when both B/H and M are small. For most cases considered, as illustrated in Figs. 9(b)-9(d), an increasing k_h makes the failure geometry deeper and wider. Additionally, comparing Figs. 9(a)-9(d), it is seen that with the increase of M, a larger failure block can be observed under both static and seismic condition. This can be ascribed to the fact that an increasing M indicates a decreasing variation ratio of c_u in the depth direction, namely the strength of soils away from the slope top surface are reduced, which makes more soils prone to failure.

As the stability number and failure mechanism are significantly affected by M and B/H, in engineering practice, using the traditional toe failure mechanism may lead to an erroneous estimate of seismic slope stability, which in turn leads to an inappropriate reinforcement scheme and reinforcement location. It clearly shows the importance of using extended failure mechanisms rather than the toe failure mechanism only in the seismic design for slopes.

7. Conclusions

This study conducts an analysis on the 3D seismic stability of slopes with linearly increasing undrained shear strength c_u. Based on the kinematic approach of limit analysis and the pseudo-static approach, the upper bound solution to the stability number N_s is obtained. The effects of c_u profile parameter M, horizontal seismic coefficient k_h and width-to-height ratio B/H on the stability and failure geometry of slopes are investigated. The key findings are outlined as follows:

• The increase of M gives rise to an increasing N_s. Slopes with smaller B/H are more sensitive to the variation of M. An increase in k_h leads to a decrease in N_s, and gentler slopes are more sensitive to the variation of k_h.

• The failure geometry is significantly affected by M and k_h. The below-toe failure can only be observed in gentle slopes when M is large, while the face failure is produced for a wide range of slope angels when M is small.

• The width-to-height ratio B/H plays a key role for soils with a large gradient in c_u in the depth direction, i.e., small value of M. A novel finding is drawn that an increase in k_h makes the failure surface shallower when B/H is small.

• This research adopted an analytical method to evaluate the 3D undrained slope stability. Further work should focus on the development of efficient methods for more complex 3D problems, to model the unsaturated conditions, complex

loading conditions and the heterogeneity of internal friction angle.

Acknowledgments

The research described in this paper was financially supported by the National Natural Science Foundation of China (Project No..: 51208301). The authors wish to express their gratitude for the above financial support.

References

Ajith, A., Francis, K.A. and Pillai, R.J. (2024), "Evaluation of pore-pressure variation and slope stability on terraced cultivation using physics-based landslide susceptibility model", *Geomorphology*., **450**, 109081. https://doi.org/10.1016/j.geomorph.2024.109081.

Azarafza, M., Bonab, M.H. and Akgun, H. (2021), "Numerical analysis and stability assessment of complex secondary toppling failures: A case study for the south pars special zone", *Geomech. Eng.,* **27**(5), 481-495. https://doi.org/10.12989/gae.2021.27.5.481.

Bhandari, T., Hamad, F., Moormann, C., Sharmai, K.G. and Westrich, B. (2016), "Numerical modelling of seismic slope failure using MPM", *Comput. Geotech.*, **75**, 126-134. https://doi.org/10.1016/j.compgeo.2016.01.017.

Bi, J.F., Luo, X.Q., Zhang, H.T. and Shen, H. (2019), "Stability analysis of complex rock slopes reinforced with prestressed anchor cables and anti-shear cavities", *Bull. Eng. Geol. Environ.*, **78**(2), 2027-2039. https://doi.org/10.1007/s10064-017-1171-8.

Bonilla-Sierra, V., Scholtes, L., Donze, F.V. and Elmouttie, M.K. (2015), "Rock slope stability analysis using photogrammetric data and DFN–DEM modelling", *Acta Geotech.*, **10**(4), 497-511. https://doi.org/10.1007/s11440-015-0374-z.

Chehade, H.A., Dias, D., Sadek, M., Jenck, O. and Chehade, F.H. (2022), "Seismic internal stability of saturated reinforced soil retaining walls using the upper bound theorem of limit analysis", *Soil Dyn. Earthq. Eng.*, **155**, 107180. https://doi.org/10.1016/j.soildyn.2022.107180.

Chen, W.F. (1975), *Limit Analysis and Soil Plasticity*, Elsevier Scientific Publishing Company, New York, NY, USA.

Chen, Z.Y. (1992), "Random trials used in determining global minimum factors of safety of slopes", *Can. Geotech. J.*, **29**(2), 225-233. https://doi. org/ 10. 1139/ t92- 026.

Chaudhary, N., Metya, S. and Sharma, K.K. (2024), "Influence of hydraulic distribution pattern on the rock slope stability under block toppling failure", *KSC J. Civ. Eng.*, **28**(4), 1253-1266. https://doi.org/10.12989/gae.2019.19.2.179.

Deng, D.P., Lu, K. and Li, L. (2019), "LE analysis on unsaturated slope stability with introduction of nonlinearity of soil strength", *Geomech. Eng.*, **19**(2), 179-191. https://doi.org/10.12989/gae.2019.19.2.179.

Feng, Z.K. and Xu, W.J. (2021), "GPU material point method (MPM) and its application on slope stability analysis", *Bull. Eng. Geol. Environ.*, **80**(7), 5437-5449. https://doi.org/10.1007/s10064-021-02265-8.

Gao, G., Meguid, M.A., Chouinard, L.E. and Zhan, W.W. (2021), "Dynamic disintegration processes accompanying transport of an earthquake-induced landslide", *Landslides.*, **18**(3), 909-933. https://doi.org/10.1007/s10346-020-01508-1.

Gap, Y.F., Zhang, F., Lei, G.H., Li, D.Y., Wu, Y.X. and Zhang, N. (2013), "Stability charts for 3D failures of homogeneous slopes", *J. Geotech. Geoenviron. Eng.*, **139**(9), 1528-1538. https://doi.org/10.1061/(ASCE)GT.1943-5606.0000866.

Griffiths, D.V. and Yu, X. (2015), "Another look at the stability of slopes with linearly increasing undrained strength", *Geotechnique*, **65**(10), 824-830. https://doi.org/10.1680/jgeot.14.T.030.

Griffiths, D.V. and Martin, C.M. (2020), "Critical failure mechanisms in relatively flat undrained slopes", *Geotech. Lett.*, **10**(2), 95-99. https://doi.org/10.1680/jgele.19.00075.

Hong-in, P., Keawsawasvong, S., Lai, V.Q., Nguyen, T.S., Tanapalungkorn, W. and Likitlersuang, S. (2023), "3D stability and failure mechanism of undrained clay slopes subjected to seismic load", *Geotech. Geol. Eng.*, **41**(7), 3941-3969. https://doi.org/10.1007/s10706-023-02497-3.

Hossley, A. and Lenshchinsky, B. (2019), "Stability and failure geometry of slopes with spatially varying undrained shear strength", *J. Geotech. Geoenviron. Eng*., **145**(5), 06019002. https://doi.org/10.1061/(ASCE)GT.1943-5606.0002046.

Huang, A.P., Zhu, Y.P., Ye, S.H., Wang, L., Peng, J.G. and Fang, G.W. (2023), "Seismic stability limit analysis of unsaturated soil slopes reinforced by frame beam anchor plates", *KSCE J. Civ. Eng.*, **27**(9), 3778-3792. https://doi.org/10.1007/s12205-023-1928-5.

Hunter, J.H. and Schuster, R.L. (1968), "Stability of simple cuttings in normally consolidated clays", *Geotechnique*, **18**(3), 372-378. https://doi.org/10.1680/geot.1968.18.3.372.

Karrech, A., Dong, X., Elchalakani, M., Basarir, H., Shahin, M.A. and Regenauer-Lieb, K. (2022), "Limit analysis for the seismic stability of three-dimensional rock slopes using the generalized Hoek-Brown criterion", *Int. J. Min. Sci. Technol*., **32**(2), 237-245. https://doi.org/10.1016/j.ijmst.2021.10.005.

Ke, L.J., Gao, Y.F., Zhao, Z.H., Zhou, Y.D. and Ji, J. (2021), "Undrained bearing capacity of strip footing near slopes considering the orientation of strength increase", *Int. J. Geomech.*, **21**(7), 06021016. https://doi.org/10.1061/(ASCE)GM.1943-5622.0002088.

Koppula, S.D. (1984), "On stability of slopes in clays with linearly increasing strength", *Can. Geotech. J.*, **21**(3), 577-581. https://doi.org/10.1139/t84-059.

Kumar, J., Chakraborty, M. and Sahoo, J.P. (2014), "Stability of unsupported vertical circular excavations", *J. Geotech. Geoenviron. Eng*., **140**(7), 04014028. https://doi.org/10.1061/(ASCE)GT.1943-5606.0001118.

Li, A.J., Merifield, R.S. and Lyamin, A.V. (2009), "Limit analysis solutions for three dimensional undrained slopes", *Comput. Geotech.*, **36**(8), 1330-1351. https://doi.org/10.1016/j.compgeo.2009.06.002.

Li, B., Zhang, F. and Wang, D. (2018), "Impact of crack on stability of slope with linearly increasing undrained strength", *Math. Probl. Eng.*, **2018**, 1096513. https://doi.org/10.1155/2018/1096513.

Mase, L.Z., Likitlersuang, S. and Tobita, T. (2020), "Verification of liquefaction potential during the strong earthquake at the border of Thailand–Myanmar", *J. Earthq. Eng.*, **26**(4), 2023-2050. https://doi.org/10.1080/13632469.2020.1751346.

Mase, L.Z., Likitlersuang, S. and Tobita, T. (2021), "Ground motion parameters and resonance effect during strong earthquake in northern Thailand", *Geotech. Geol. Eng.*, **39**(3), 2207-2210. https:// doi. org/ 10.1007/ s10706- 020- 01619-5.

Mase, L.Z., Tanapalungkorn, W., Likitlersuang, S., Ueda, K. and Tobita, T. (2022), "Liquefaction analysis of Izumio sands under variation of ground motions during strong earthquake in Osaka", *Soils Found.*, **62**(5), 101218. https://doi.org/10.1016/j.sandf.2022.101218.

Mase, L.Z., Tanapalungkorn, W., Anussornrajkit, P. and Likitlersuang, S. (2024), "Assessing liquefaction risk and hazard mapping in a high-seismic region: a case study of Bengkulu City, Indonesia", *Nat. Hazards*, **Online**.

https://doi.org/10.1007/s11069-024-07057-3.
Michalowski, R.L. (2002), "Stability charts for uniform slopes", *J. Geotech. Geoenviron. Eng.*, **128**(4), 351-355. https://doi.org/10.1061/(ASCE)1090-0241(2002)128:4(351).
Michalowski, R.L. and Drescher, A. (2009), "Three-dimensional stability of slopes and excavations", *Geotechnique*, **59**(10), 839-850. https://doi.org/10.1680/geot.8.P.136.
Naeij, M., Ghasemi, H., Ghafarian, D. and Javanmardi, Y. (2021), "Explicit finite element analysis of slope stability by strength reduction", *Geomech. Eng.*, **26**(2), 133-146. https://doi.org/10.12989/gae.2021.26.2.133.
Petchkaew, P., Keawsawasvong, S., Tanapalungkorn, W. and Likitlersuang, S. (2023a), "3D stability analysis of unsupported rectangular excavation under pseudo-static seismic body force", *Geomech. Geoeng.*, **18**(3), 175-192. https://doi.org/10.1080/17486025.2021.2019321.
Petchkaew, P., Keawsawasvong, S., Tanapalungkorn, W. and Likitlersuang, S. (2023b), "Seismic stability of unsupported vertical circular excavations in *c-φ* soil", *Transp. Infrastruct. Geotechnol.*, **10**(2), 165-179. https://doi.org/10.1007/s40515-021-00221-3.
Qin, C.B., Chian, S.C. and Yu, J. (2018), "Stability analysis of initial collapse and earthquake-induced secondary failure using discretization-based kinematic analysis", *Int. J. Gemech.*, **18**(11), 04018155. https://doi.org/10.1061/(ASCE)GM.1943-5622.0001304.
Park, D. and Michalowski, R.L. (2018), "Intricacies in three-dimensional limit analysis of earth slopes", *Int. J. Numer. Anal. Methods Geomech*., **42**(17), 2109-2129. https://doi.org/10.1002/nag.2846.
Rao, P.P., Wu, J., Jiang, G.Y., Shi, Y.W., Chen, Q.S. and Nimbalkar, S. (2021), "Seismic stability analysis for a two-stage slope", *Geomech. Eng.*, **27**(2), 189-196. https://doi.org/10.12989/gae.2021.27.2.189.
Ray, R., Deb, K. and Shaw, A. (2019), "Pseudo-Spring smoothed part icle hydrodynamics (SPH) based computational model for slope failure", *Eng. Anal. Bound. Elem.*, **101**, 139-148. https://doi.org/10.1016/j.enganabound.2019.01.005.
Satyanaga, A., Moon, S.W. and Kim, J.R. (2022), "Stability analyses of dual porosity soil slope", *Geomech. Eng.*, **28**(1), 77-87. https://doi.org/10.12989/gae.2021.28.1.077.
Shi, Y.W., Luo, X.Q. and Wang, P.F. (2022), "Three-dimensional stability assessment of slopes with spatially varying undrained shear strength", *Geomech. Eng.*, **31**(4), 375-384. https://doi.org/10.12989/gae.2022.31.4.375.
Shu, S., Ge, B., Wu, Y.X. and Zhang, F. (2023), "Probabilistic assessment on 3D stability and failure mechanism of undrained slopes based on the kinematic approach of limit analysis", *Int. J. Geomech.*, **23**(1), 06022037. https://doi.org/10.1061/(ASCE)GM.1943-5622.0002635.
Tran, A.T.P., Kim, A.R. and Cho, G.C. (2019), "Numerical modeling on the stability of slope with foundation during rainfall", *Geomech. Eng.*, **17**(1), 109-118. https://doi.org/10.12989/gae.2019.17.1.109.
Tran, A.T.P., Cho, Y., Seo, H. and Kim, B. (2023), "Seismic fragility assessments of fill slopes in South Korea using finite element simulations", *Geomech. Eng.*, **32**(4), 341-380. https://doi.org/10.12989/gae.2023.34.4.341.
Ukritchon, B., Yoang, S. and Keawsawasvong, S. (2020), "Undrained stability of unsupported rectangular excavations in non-homogeneous clays", *Comput. Geotech.*, **117**, 103281. https://doi.org/10.1016/j.compgeo.2019.103281.
Wang, L., Sun, D.A. and Li, L. (2019), "3D stability of partially saturated soil slopes after rapid drawdown by a new layer-wise summation method", *Landslides.*, **16**(2), 295-313. https://doi.org/10.1007/s10346-018-1081-2.
Wang, Y.K., Shang, H.W., Wan, Y.K. and Yu, X. (2024), "Reliability analysis of soil slope reinforced by micro-pile considering spatial variability of soil strength parameters", *Geomech. Eng.*, **36**(6), 631-640. https://doi.org/10.12989/gae.2024.36.6.631.
Wang, J.H. and Xu, WJ. (2025), "Slope stability and failure dynamics of rainfall-induced landslide: Algorithm and applications", *Gomput. Geotech.*, **177**, 106919. https://doi.org/10.1016/j.compgeo.2024.106919.
Weng, M.C., Lin, M.L., Lo, C.M., Li, H.H., Lin, C.H., Lu, J.H. and Tsai, S.J. (2019), "Evaluating failure mechanisms of dip slope using a multiscale investigation and discrete element modelling", *Eng. Geol.*, **263**, 105303. https://doi.org/10.1016/j.enggeo.2019.105303.
Yang, X.L. and Li, Z.W. (2018), "Comparison of factors of safety using a 3D failure mechanism with kinematic approach", *Int. J. Geomech.*, **18**(9), 04018107. https://doi.org/10.1061/(ASCE)GM.1943-5622.0001235.
Yang, X.L. and Pan, Q.J. (2015), "Three dimensional seismic andstatic stability of rock slopes", *Geomech. Eng.*, **18**(1), 97-111. https://doi.org/10.12989/gae.2015.8.1.097.
Zhang, F., Leshchinsky, D., Baker, R., Gao, Y.F. and Leshchinsky, B. (2016), "Implications of variationally derived 3D failure mechanism", *Int. J. Numer. Anal. Method. Geomech.*, **40**(18), 2514-2531. https://doi.org/ 10.1002/nag.2543.
Zhang, X.Q., Song, X., Wu, S.C. and Zhong, G. (2024), "Meshless analysis method for the whole process of progressive failure of slope", *Indian Geotech. J.*, **54**(2), 500-513. https://doi.org/10.1007/s40098-023-00787-4.
Zhou, Y., Zhang, F. and Li, B. (2019), "Static and seismic stability charts for three-dimensional cut slopes and natural slopes under short-term undrained conditions", *Adv. Civ. Eng.*, **2019**, 191467. https://doi.org/10.1155/2019/1914674.
Zhou, J.F and Qin, C.B. (2020), "A novel procedure for 3D slope stability analysis: lower bound limit analysis coupled with block element method", *Bull. Eng. Geol. Environ.*, **79**(4), 1815-1829. https://doi.org/10.1007/s10064-019-01657-1.

GC